

Crystallization Kinetics of Se-Te-S Ternary-Component Chalcogenide Glasses Using Non-Isothermal DSC

A. A. El-Sharkawy, M. T. Dessouky and A. Raafat.

Department of Physics, Faculty of Science, Al-Azhar University, Cairo, Egypt.

Received: 21 Feb. 2015, Revised: 22 Mar. 2015, Accepted: 24 Mar. 2015.

Published online: 1 Jul. 2015.

Abstract: The crystallisation kinetics of bulk $\text{Se}_{85-x}\text{Te}_{15}\text{S}_x$ ($x = 5, 10, 15, 20$ and 25 at. %) ternary-component chalcogenide glasses have been studied using differential scanning calorimetry with different heating rates ($\beta = 5, 10, 20, 30, 40$ K/min). The studied alloy exhibited overlapping exothermic peaks which were deconvoluted using a Gaussian fitting of two peaks, making it possible to study the crystallization phases separately. The glass transition activation energy E_g and the crystallization activation energies for the first and the second crystallization peaks (E_{c1} and E_{c2}) have been identified. The determined kinetic parameters have made it possible to postulate the type of crystal growth exhibited in the crystallization process. The phases at which the alloy crystallizes after the thermal process have been identified by X-ray diffraction. The diffractogram of the transformed material indicates the presence of microcrystallites of $\text{Se}_{7.68}\text{Te}_{0.32}$ and S_5Se_4 , with a remaining additional amorphous matrix.

1 Introduction

Chalcogenide glasses are a recognized group of inorganic glassy materials which always contain one or more of the chalcogen elements Se, S or Te. They are generally less robust, weaker bounded materials than oxide glasses [1]. Chalcogenide glasses have been attracting much attention in the field of electronics as well as in infrared optics, since they exhibit several peculiar phenomena useful for devices such as electrical switches, memories, image storage, and photo resistors. The common feature of these glasses is the presence of localized states in the mobility gap, as the result of the absence of long-range order as well as various inherent defects. Optical data storage based on laser induced amorphous to crystalline (a-c) phase transformation of chalcogenide glasses is an area with on-going research activity [2-9]. The trend of using amorphous semiconducting materials, rather than carefully prepared crystalline semiconductors. Differential scanning calorimetry (DSC) is one of the tools for studying crystallization kinetics, as has been widely discussed in the literature [10-14]. Thermally activated transformations in the solid state can be investigated by isothermal or non-isothermal experiments [15-17]. In the isothermal method, the sample is brought quickly to a temperature above the glass transition temperature (T_g) and the heat evolved during the crystallization process is recorded as a function of time. In the non-isothermal method, the sample is heated at a fixed rate and the heat evolved is again

recorded as a function of temperature or time. A disadvantage of the isothermal technique is the impossibility of reaching a test temperature instantaneously and, during the time in which the system needs to stabilize, no measurements are possible. A constant heating rate experiment does not have this drawback [18]. It is of interest to find the crystallization kinetics using different methods for a single alloy. In the present work crystallization kinetics of $\text{Se}_{85-x}\text{Te}_{15}\text{S}_x$ ($x = 5, 10, 15, 20$ and 25 at. %) ternary-component chalcogenide glasses have been investigated under non-isothermal conditions, the nucleation and growth morphology have been determined through the JMA model. Also other kinetic parameters like activation energy of crystallization and activation energy for glass transition have been determined. Identification of the phases at which the alloys crystallize after thermal process has been proposed using X-rays diffraction.

2 Experimental Details

High purity (99.999%) Se, Te and S elements (5N, Aldrich and Sigma chemical company) were weighed in appropriate atomic weight percent proportions using an electronic balance. The materials were evacuated in silica ampoules of long length 15 cm and internal diameter 12 mm in order to avoid the expansion and burst of the sulphur.

The ampoules were sealed under a vacuum of 10^{-5} Torr to

*Corresponding author e-mail:

remove the possibility of any reaction of alloys with oxygen at high temperature. The ampoules were heated in an electronic furnace at the rate of 3 – 4 K/min up to 1123K for 10–12 h. The synthesis was performed in a programmable rocking furnace and slowly heated up to approximately 950 °C with the temperature ramp about 5 °C/min, for about 24 h. During the melt process, the ampoule was inverted at regular time intervals (~ 1 h) so that the amorphous solid will be homogenous and isotropic. After the synthesis, the melt was quenched rapidly in ice water at 273 K to obtain the Se-Te-S glassy alloy. Then the solid was broken along its natural stress line into smaller pieces suitable for grinding. The elemental composition of the samples was analyzed by using energy dispersive X-ray spectrometer unit (EDXS) interfaced with a scanning electron microscope, SEM (JOEL XL) operating an accelerating voltage of 30 kV. The relative error of determining the indicated elements does not exceed 4%. X-ray powder diffraction (XRD) Philips diffractometry (1710), with Cu-K α 1 radiation ($\lambda = 1.54056 \text{ \AA}$) have been used to examine the amorphous nature of the Se_{85-x}Te₁₅S_x (x = 5, 10, 15, 20 and 25 at. %) compositions. The non-crystalline nature of each alloy was confirmed using X-ray diffraction (XRD) as shown in Fig. 1.

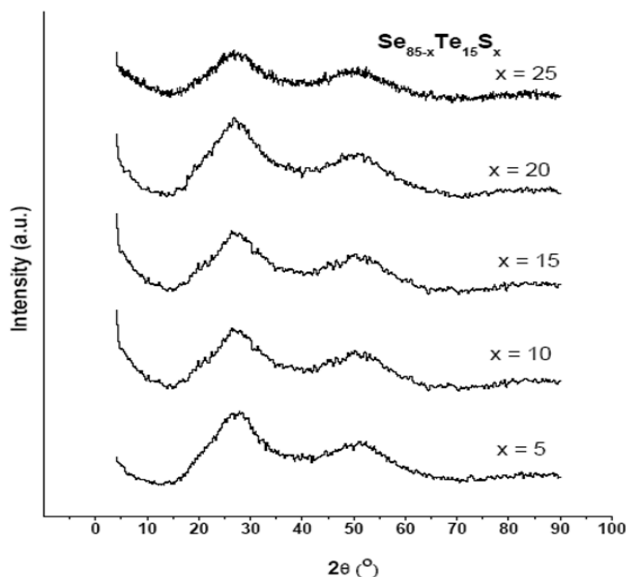


Fig. 1: X-ray diffraction patterns of amorphous Se_{85-x}Te₁₅S_x (x = 5, 10, 15, 20 and 25 at. %) as prepared samples.

The calorimetric measurements were carried out in a differential scanning calorimeter Shimadzu 50 with an accuracy of ± 0.1 K. The calorimeter was calibrated, for each heating rate, using well-known melting temperatures and melting enthalpies of zinc and indium supplied with the instrument. Twenty mg powdered samples, crimped into aluminum pans, were scanned at different heating rates ($\beta = 5, 10, 20, 30, 40$ K/min). The temperatures of the glass transition, T_g , the crystallization extrapolated onset, T_{in} , the

crystallization peak, T_p and the melting temperature T_m were determined with an accuracy of ± 1 K.

3 Result and Discussion

The X-ray diffraction patterns of Se_{85-x}Te₁₅S_x (x = 5, 10, 15, 20, 25 at. %) as prepared samples are shown in Fig. 1, the absence of any sharp peaks emphasizes the glassy nature of these compositions. For further interpretation of the patterns, these amorphous samples had two main diffraction humps of the pure Se₈₀Te₂₀ and doped Se_{85-x}Te₁₅S_x (x = 5, 10, 15, 20, 25) samples. The X-ray intensity data were collected in the angular ranges $2\theta = 4$ -90 degrees. The presence of two amorphous humps may be interpreted in terms of finding of two amorphous phases of glass.

3.1.1 Compositional dependence of activation energies for glass transition E_g and for crystallization E_c

In order to investigate crystallization kinetics of Se_{85-x}Te₁₅S_x (x = 5, 10, 15, 20, 25) chalcogenide glasses, DSC experiments were carried out at different heating rates from 5-40 K/min.

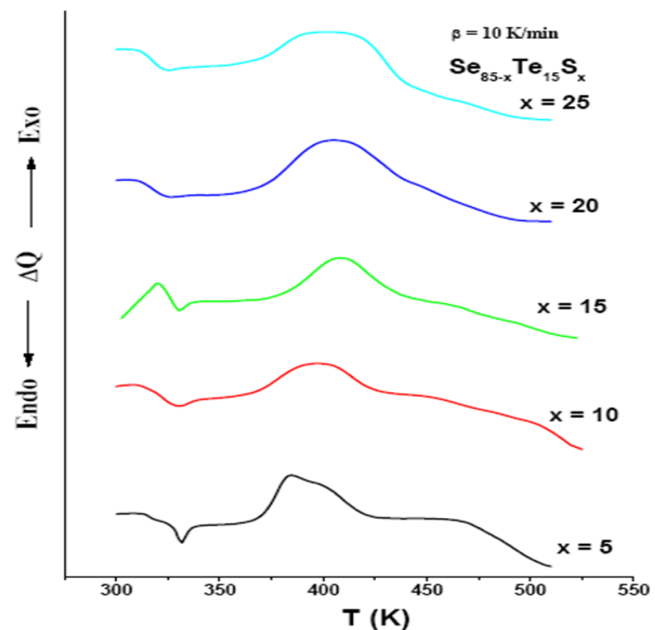


Fig. 2: The DSC traces of the as prepared Se_{85-x}Te₁₅S_x compositions (x = 5, 10, 15, 20 and 25 at. %) at heating rate $\beta = 10$, K/min.

Fig. 2 shows the DSC traces of the as prepared Se_{85-x}Te₁₅S_x compositions (x = 5, 10, 15, 20, 25) at heating rate $\beta = 10$ K/min. Fig. 3 shows the DSC traces of Se₈₀Te₁₅S₅ at different heating rate extended from 5 to 40 K/min. Fig. 4 shows the DSC traces for Se₈₀Te₁₅S₅ glass at heating rate 10 K/min, this figure displays at first an endothermic peak, which at its beginning the glass transition temperature T_g

can be determined, secondly it is clearly regarding an exothermic peak, its beginning represent the initial temperature of crystallization T_i , its peak represent the crystallization temperature T_p , at its end represent the T_f temperature at which crystallization completed. A broadening in the crystallization peak observed which consists of two overlapped crystallized peaks, so dividing it into two peaks was necessary. The Separation of two overlapped crystallized peaks is shown in the inset of Fig. 4. The indices 1 and 2 in T_{p1} and T_{p2} denote to the first peak and the second peak respectively.

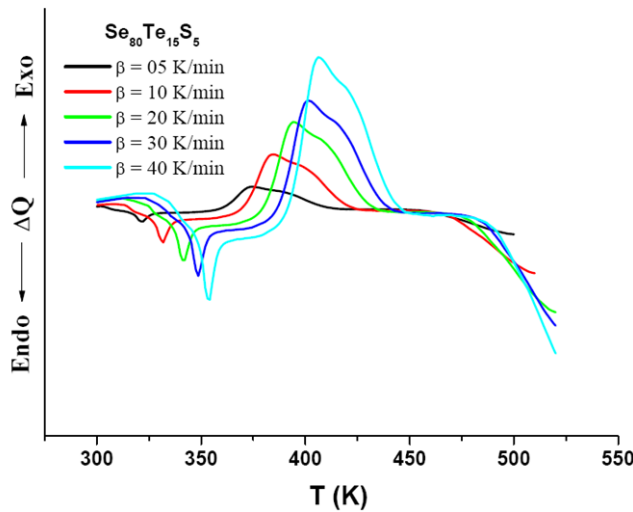


Fig. 3: The DSC traces of the as prepared $Se_{80}-Te_{15}-S_5$ composition at different heating rates ($\beta = 5, 10, 20, 30$ and 40 K/min)

From the DSC traces of various compositions of $Se_{85-x}-Te_{15}-S_x$ chalcogenide glass, it is clearly observed that there is a decreasing in T_g with increasing S content, also T_g increases gradually with increasing the heating rate for each specimen.

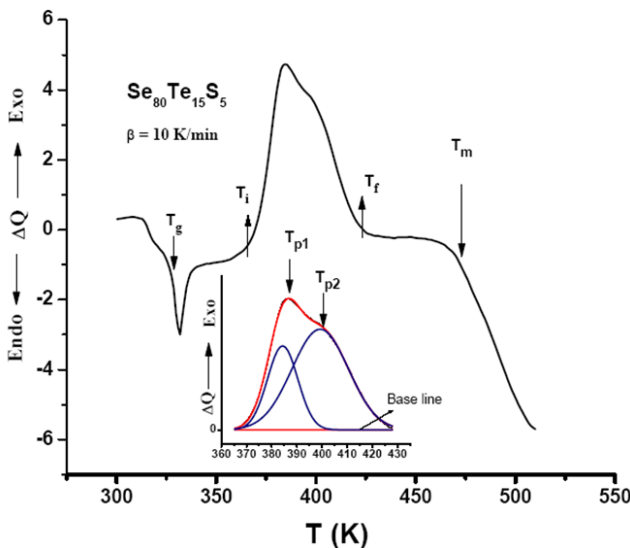


Fig. 4: DSC traces for $Se_{80}-Te_{15}-S_5$ chalcogenide glass heating rate 10 K/min, the inset represents separation of two overlapped crystallized peaks.

Fig. 4 shows the variation of T_g with S content within the compositions at different heating rates. This decreasing of T_g with increasing S contents within the composition can be understood in terms of the density of the elements that formed the composition, hence Sulfur is less denser than selenium which decrease the average density of the composition by replacing of Selenium atoms with sulfur atoms. Table (1) represents the physical properties of the constituting elements of $Se_{85-x}-Te_{15}-S_x$ composition.

Table 1: Physical parameters of the constituent elements

Property	Se	Te	S
Density (g/cc)	4.79	6.24	2.067
Coordination number	2	2	2
Atomic radius (Å)	1.22	1.42	1.09
Electronegativity	2.55	2.1	2.58
Bond energy (Kcal mol ⁻¹)	44.04	33	55
Heat of atomization (kcal/g/atom)	49.4	46	60.65

The activation energy of glass transition was determined using the values of T_g according to their corresponding heating rates across Kissinger relation, which basically derived for the crystallization process and suggested to be valid for the glass transition [19]. This relation is given by:

$$\ln\left(\frac{T_g^2}{\beta}\right) = \frac{E_g}{RT_g} + const \quad (1)$$

Where R is the universal gas constant. Fig. (6) Shows the relation between $\ln\left(\frac{T_g^2}{\beta}\right)$ versus $(1/T_g)$. The values of E_g obtained from the slope of the straight line corresponding to each specimen. These values give decreasing trend of E_g with increase S contents (as shown in Fig. (7)). The decreasing of E_g result in the decreasing of T_g .

According to the DSC traces of and the crystallization region which was divided in two peaks, the values of T_p was taken according to the two overlapped peaks, then drawn with the variation of Sulfur contents within the composition at different heating rates. Fig (8.a) and Fig (8.b) show the variation of T_p with S contents at different heating rates according to the first peak and the second peak respectively. It was clear that T_p increases with increasing the heating rate, this trend observed for the two overlapped peaks. T_p also increases with increasing S contents (at $x = 0, 5, 10, 15, 20$) then drop suddenly when reach to $x = 25$.

For the evaluation of the activation energy of crystallization E_c , using the variation of T_p with the heating rate β according to the Kissinger relation [19] which modified by Vazquez et al [20] for non-isothermal analysis as follows

$$\ln\left(\frac{T_p^2}{\beta}\right) = \frac{E_c}{RT_p} + \ln\left(\frac{E_c}{RK_0}\right) \quad (2)$$

From the experimental data, a plot of $\ln(T_p^2/\beta)$ versus $1/T_p$ has been drawn for different compositions showing the straight regression line in Fig. 9 (a, b) according to the first peak and second peak respectively. The activation energy, E_c and the frequency factor, K_o are then evaluated by least squares fitting method of the last equation.

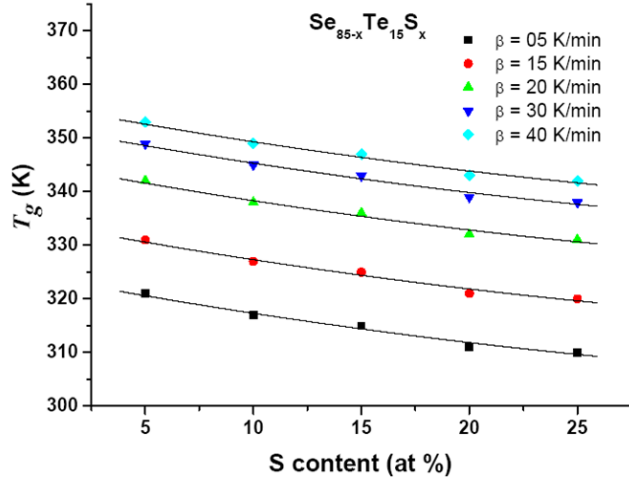


Fig. 5: The variation of T_g against S content at different heating rates for the $Se_{85-x}Te_{15}S_x$ compositions

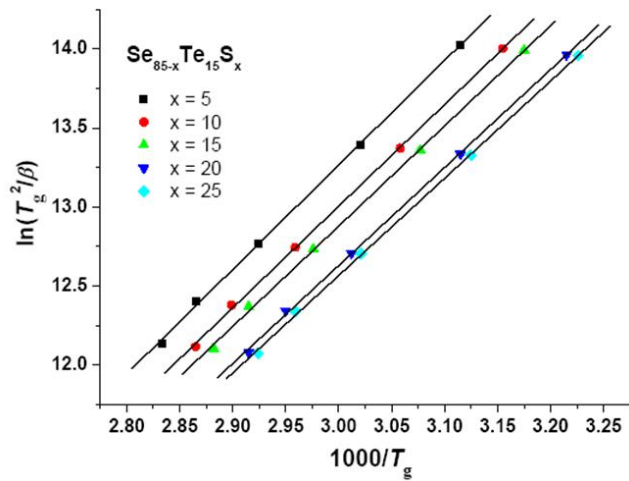


Fig. 6: The relation between $\ln(T_g^2/\beta)$ versus $(1/T_g)$ for the $Se_{85}Te_{15}S_x$ ($x = 5, 10, 15, 20, 25$)

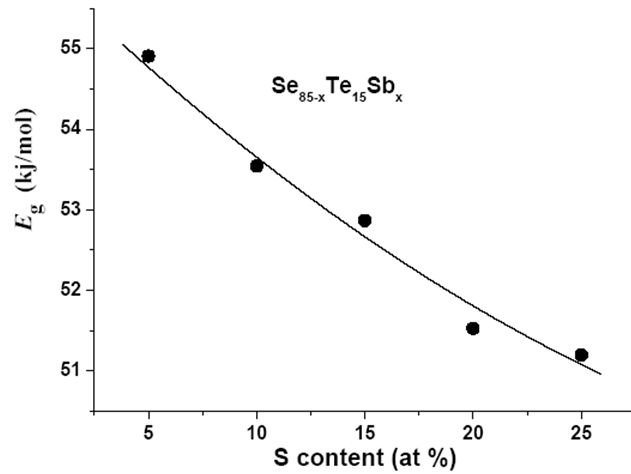


Fig. 7: The values of the activation energies E_g of glass transition as a function of S content.

Fig. 10 (a, b) shows the values of E_c and K_o as a function of S content according to the first peak and second peak respectively. The frequency factor, K_o , (which measure the probability of effective molecular collisions for the formation of the activated complexes in each case) increases with increasing S content reaching to the value $x = 20$ and then decrease at $x = 25$.

Also it is observed that E_c increase with increasing Sulfur content within the composition until reaching to the value of $x = 20$ and then decrease at $x = 25$. The trend of the activation energy can be interpreted in term of the bond energies. In view of the chemical bond approach to examine the structure and properties of various types of chalcogenide glasses, atoms combine more favorably with atoms of different kinds than with the same kind; this assumption which is generally found to be valid for glass structures, has been used by Zachariasen [21] in his covalently bonded continuous random network model. On using this assumption, bonds between like atoms will only occur if there is an excess of a certain type of atoms. Bonds are formed in the sequence of decreasing bond energies until all available valences for the atoms are saturated.

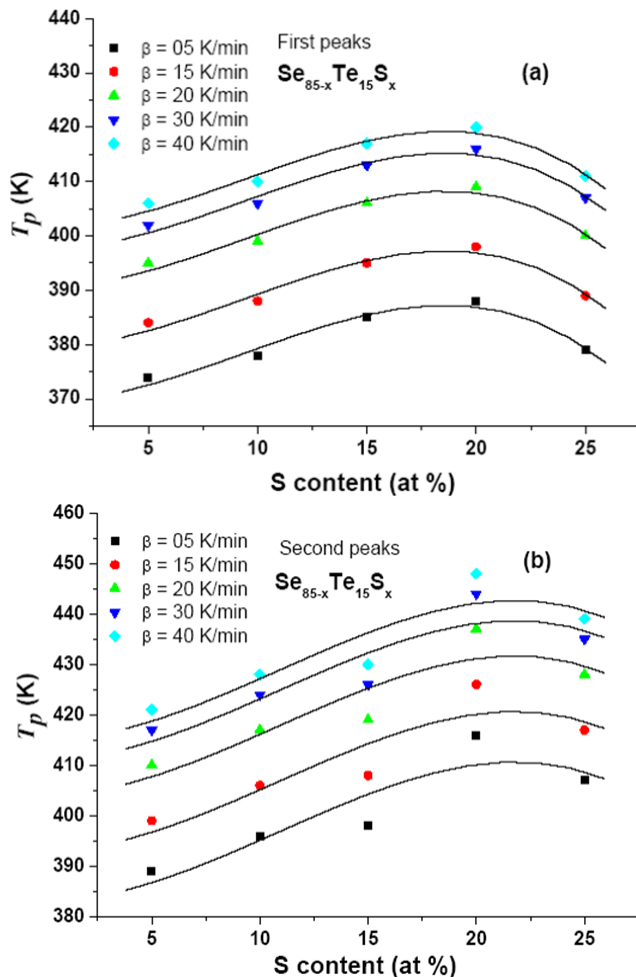


Fig. 8: A plot of T_p versus S contents of the $\text{Se}_{85}\text{Te}_{15}\text{S}_x$ chalcogenide glass at different heating rates according to (a) the first peak of crystallization and (b) the second peak of crystallization.

The bond energies $D(A-B)$ for heteronuclear bonds have been calculated by using the relation [22]

$$D(A-B) = [D(A-A) \times D(B-B)]^{1/2} + 30(\chi_A - \chi_B)^2 \quad (3)$$

Where $D(A-A)$ and $D(B-B)$ are the energies of the homonuclear bonds, χ_A and χ_B are electronegativity values for atoms involved. Both the electronegativity and the homonuclear bonds $D(A-A)$ and $D(B-B)$ for Te, Se and S are listed in table (1). The types of bonds expected to occur in the system under investigation are S-Te bonds (49.515 kcal/mol), S-Se (49.243 kcal/mol) and Se-Se (44.04 kcal/mol). In the present compositions the S atoms strongly bond to Te. The S-Te bonds have the highest probability to form, then the S-Se bonds. After these bonds are formed, there are still unsatisfied Se valences, which are much satisfied by the formation of Se-Se bond. Knowing the bond energies, the cohesive energy (CE) have been derived by assuming the bond energies over all the bond expected in the system under test by the following equation

$$CE = \sum C_i D_i / 100 \quad (4)$$

Where C_i and D_i are the number of expected chemical bonds and the energy of each corresponding bond. The results of CE are listed in table (2).

Table. 2: The cohesive energy CE , the average heat of atomization H_s and the average density ρ_s as a function of S content of the $\text{Se}_{85-x}\text{Te}_{15}\text{S}_x$ glassy compositions.

S contents	CE	H_s	ρ_s
5	2.003	49.452	4.871
10	2.026	50.015	4.735
15	2.048	50.578	4.599
20	2.071	51.14	4.463
25	2.093	51.703	4.327

It should be mentioned that the approach of the chemical bond neglects dangling bond and other valence defects as a first approximation. Also van der Waals interactions are neglected, which can provide a means for further stabilization by the formation of much weaker links than regular covalent bonds.

In order to complete the vision of the chemical bonds, it is appropriate to obtain the average heat of atomization H_s , which is defined as a direct measure of cohesive energy and considered as the average bond strength. For a compound $A_x B_y C_z$, it can be calculated, in kcal/g/atom as the formula [23].

$$H_s = \frac{\alpha H_s^A + \beta H_s^B + \gamma H_s^C}{x + y + z} \quad (5)$$

where H_s^A , H_s^B , H_s^C are the heat of atomization of the involved elements (Se, Te, S) as shown table (1) and x , y , z are the ratios of these elements in the chalcogenide glass system, respectively.

The values of H_s for the Se-Te-S glass are shown in table (2). These obtained results of cohesive energy and the average heat of atomization reflect the reason behind the increasing of activation energy of crystallization with increasing of Sulfur content within the composition until reaching to the value of $x = 20$. While the drop of E_c at $x = 25$ can be interpreted as that, at a further adding of sulfur, the decreasing of the average density of the composition begin to introduce its effect on the activation energy trend

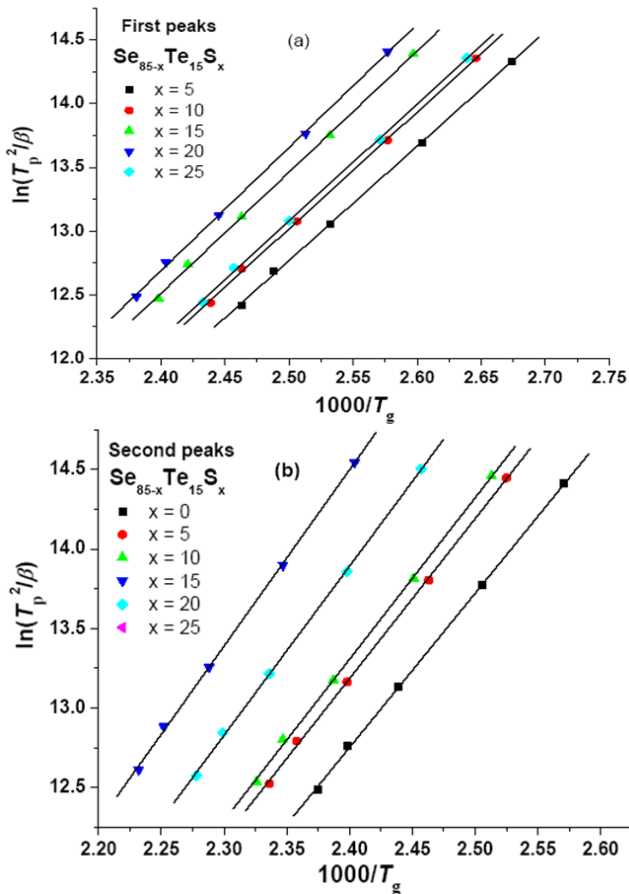


Fig. (9a): Plots of $\ln(T_p^2/\beta)$ versus $(1/T_p)$ of $\text{Se}_{85-x}\text{Te}_{15-x}\text{S}_x$ ($x = 5, 10, 15, 20, 25$) glassy alloys for both (a) the first peak and (b) the second peak beside the straight regression lines for all these alloys.

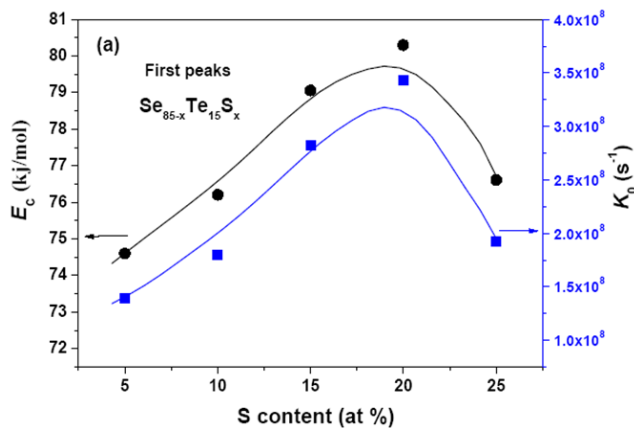


Fig. 10a: The values of the activation energies E_{c1} and the frequency factors K_{01} as a function of S content according to the first peak.

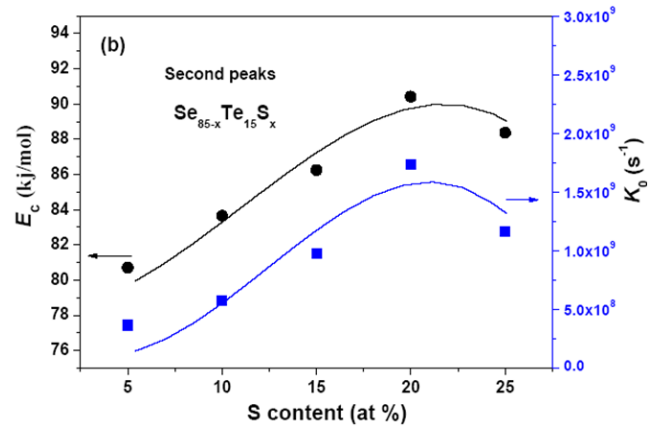


Fig. 10b: The values of the activation energies E_{c2} and the frequency factors K_{02} as a function of S content according to the second peak.

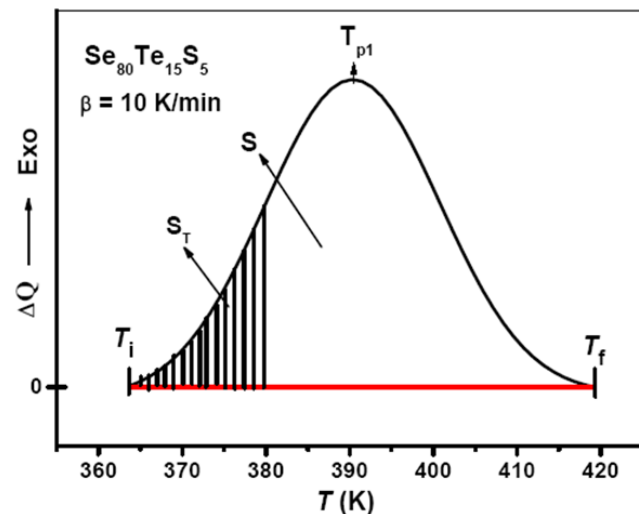


Fig. 11: DSC traces for of $\text{Se}_{80}\text{Te}_{15}\text{S}_5$ chalcogenide glass at heating rate 10 K/min, the lined area S_T shows between T_i and T_f of the peak. T_i and T_f and T according to the text

3.2 Crystallization rate and Avrami index

According to aforementioned theory of transformation kinetics as developed by Johnson and Mehl [24] and Avrami [25], an interpretation of DSC results was provided. The crystallized fraction x at a temperature T is given by $x = S_T/S$, where S is the total area of the exothermic peak between T_i (the initial temperature of crystallization) and T_f (the temperature at which crystallization is completed), S_T is the area between T_i and T , as shown in Fig.11 for the $\text{Se}_{80}\text{Te}_{15}\text{S}_5$ composition.

The graphical representation of the crystallized volume fraction, shows the typical sigmoid curve as a function of temperature for different heating rates for the first crystallization curve of $\text{Se}_{80}\text{Te}_{15}\text{S}_5$ [Fig. 12 (a, b)] based on mentioned work elsewhere [26-29]. The theoretical basis

for the interpreting of the DSC results is provided by the formal theory of transformation kinetics as developed by Johnson and Mehl [27] and Avrami [28-29]. The ratio between the ordinates of the DSC curve and the total area of the peak gives the corresponding crystallization rates,

which makes it possible to build the curves of the exothermal peaks depicted in Fig. 12 a, b for two crystallized peaks of $\text{Se}_{80}\text{Te}_{15}\text{S}_5$. It was observed that, the values of $(d\chi/dt)_p$ increase with the increase in the heating rate [30-34].

Table 3: Maximum crystallization rate $(d\chi/dt)$, kinetic exponent n and average kinetic exponent $\langle n \rangle$ of first peak for $\text{Se}_{85-x}\text{Te}_{15}\text{S}_x$ ($5 \leq x \leq 25$) alloys with different heating rates β .

x	0		5		10		15		20		25	
	$(d\chi/dt) \times 10^{-3} \text{ s}^{-1}$	n										
β (K/min)												
5	1.981	1.002	2.041	1.033	2.115	1.07	2.175	1.1	2.258	1.142	2.183	1.104
10	3.751	1.001	3.869	1.031	4.012	1.069	4.129	1.099	4.288	1.141	4.14	1.103
20	7.107	1.004	7.333	1.035	7.608	1.072	7.838	1.102	8.142	1.144	7.852	1.106
30	10.28	1.003	10.61	1.033	11.01	1.071	11.35	1.101	11.8	1.143	11.37	1.105
40	13.4	1.001	13.84	1.031	14.37	1.069	14.82	1.099	15.4	1.141	14.83	1.103
$\langle n \rangle$		1.002		1.033		1.07		1.1		1.142		1.104

Table 4: Maximum crystallization rate $(d\chi/dt)$, kinetic exponent n and average kinetic exponent $\langle n \rangle$ of second peak for $\text{Se}_{85-x}\text{Te}_{15}\text{S}_x$ ($5 \leq x \leq 25$) alloys with different heating rates β .

x	0		5		10		15		20		25	
	$(d\chi/dt) \times 10^{-3} \text{ s}^{-1}$	n										
β (K/min)												
5	1.847	1.001	1.886	1.032	1.926	1.069	2.034	1.1	1.963	1.141	1.892	1.103
10	3.505	1	3.581	1.031	3.662	1.068	3.868	1.099	3.741	1.14	3.601	1.102
20	6.651	1.003	6.802	1.034	6.961	1.071	7.355	1.102	7.128	1.143	6.854	1.105
30	9.629	1.002	9.854	1.033	10.09	1.07	10.66	1.101	10.35	1.142	9.944	1.104
40	12.57	1	12.87	1.031	13.18	1.068	13.93	1.098	13.53	1.14	12.99	1.102
$\langle n \rangle$		1.001		1.032		1.069		1.099		1.141		1.103

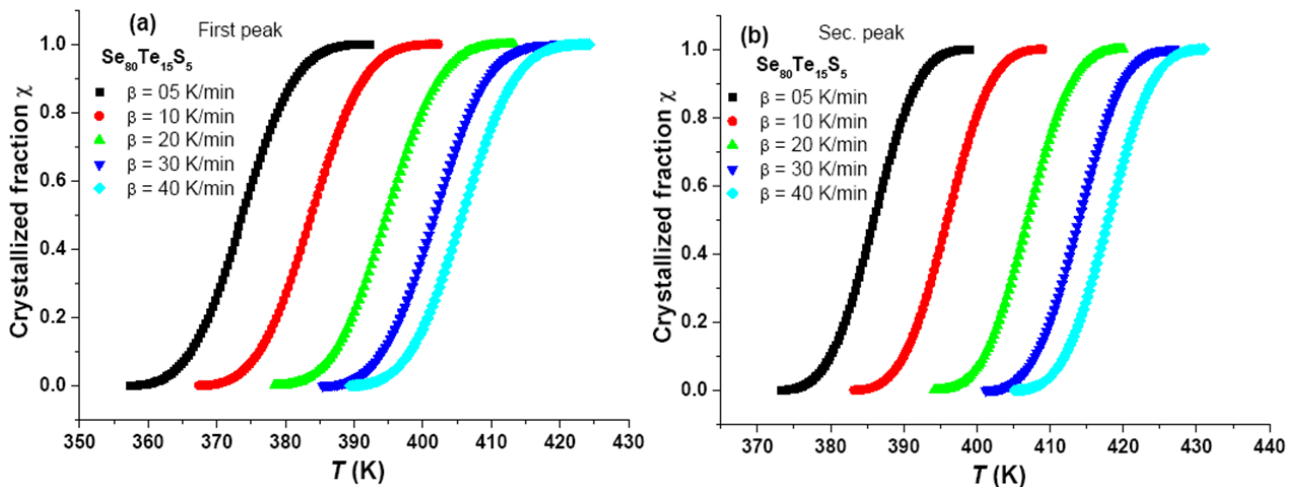


Fig. 12: Crystallized fraction χ as a function of temperature for (a) the first peak and (b) second peak of $\text{Se}_{80}\text{-Te}_{15}\text{-S}_5$ semiconductor chalcogenide glass at different heating rates.

From the experimental values of $(d\chi/dt)_p$ (listed in table (3) and table (4) for the two deconvolution peaks and using the values of activation energies E_c , one can calculate the kinetic exponent n by using the following Equation

$$\left(\frac{d\chi}{dt} \right)_p = n(0.37\beta E_c)/(RT_p^2) \quad (4)$$

The mean values, $\langle n \rangle$ of both for the first and second peaks are listed in Table 3 and table 4, respectively. Allowing for experimental error, the value of $\langle n \rangle$ is close to 1 for both the first and the second peaks. The kinetic exponent was deduced based on the mechanism of crystallization [31].

The kinetic exponent was deduced on the basis of the mechanism of crystallization [35]. According to Mahadevan *et al* [36], n may be 4, 3, 2, or 1, which are related to the different glass-crystal transformation mechanisms: $n = 4$, volume nucleation, three-dimensional growth; $n = 3$, volume nucleation, two dimensional growth; $n = 2$, volume nucleation, one dimensional growth; $n = 1$, surface nucleation, one dimensional growth from surface to the inside. Therefore, bearing in mind the above obtained mean value, $\langle n \rangle = 1$ means surface nucleation, one dimensional growth from surface to the inside.

3.3 Identification of crystalline phases by thermal treatment using X-ray diffraction

The X-ray diffraction patterns of $\text{Se}_{80}\text{Te}_{15}\text{S}_5$, $\text{Se}_{70}\text{Te}_{15}\text{S}_{15}$ and $\text{Se}_{60}\text{Te}_{15}\text{S}_{25}$ alloys annealed at temperatures beyond the peak of crystallization temperatures with a heating rate of 10 K min^{-1} for 2 h are shown in Fig. 14.

The diffractogram of the transformed material after the crystallization process suggests the presence of microcrystallites of two crystalline phases as shown in Fig. 14. From the JCPDS files these peaks can be identified as, 1- Selenium Telluride, $\text{Se}_{7.68}\text{Te}_{0.32}$ (01-087-2413) which crystallizes in the Monoclinic system with lattice parameters $a = b = 0.9103 \text{ nm}$, $c = 1.1661 \text{ nm}$ and 2- Sulfur Selenium, S_5Se_4 (card No. 01-073-1218), which crystallizes in the Hexagonal structure with lattice parameters $a = b = 0.785 \text{ nm}$ and $c = 0.462 \text{ nm}$, while there remains also an additional amorphous phase as shown in Fig. 14.

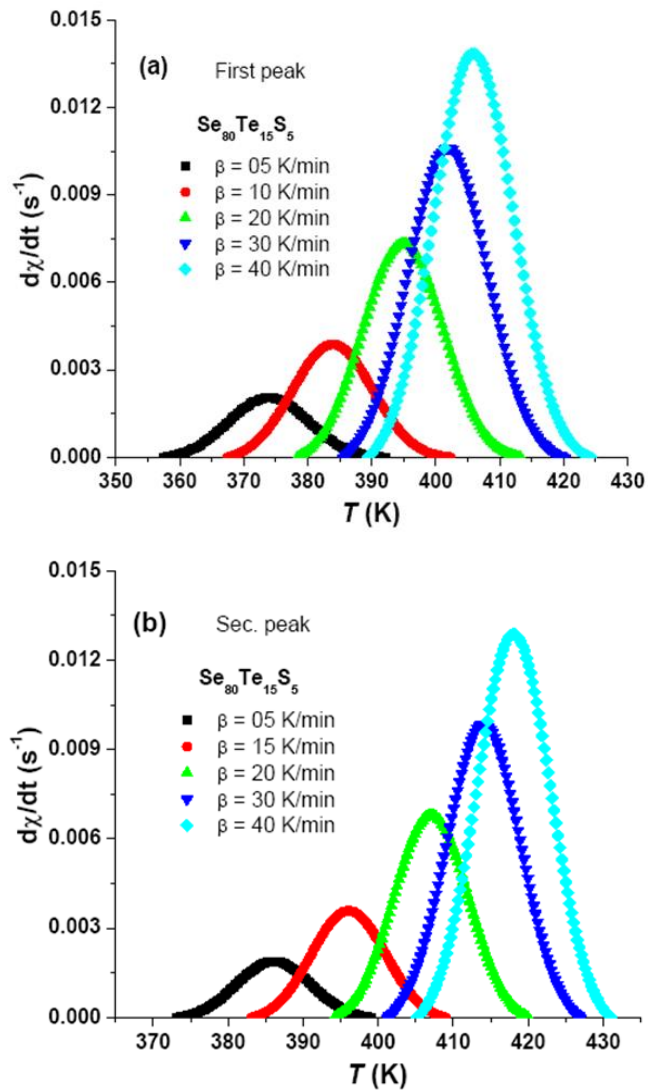


Fig. 13: Crystallized rate ($d\chi/dt$) as a function of temperature for (a) the first peak and (b) second peak of $\text{Se}_{80}\text{-Te}_{15}\text{-S}_5$ chalcogenide glass at different heating rates.

4. Conclusions

Crystallization kinetics study of the $\text{Se}_{85-x}\text{-Te}_{15}\text{-S}_x$ ($x = 5, 10, 15, 20,$ and 25) glassy compositions have resulted in the following:

1- The glass transition temperature, activation energy of glass transition and activation energy of crystallization were increases with increasing S content reaching to the value $x = 20$ and then decrease at $x = 25$. This behavior can be interpreted in terms of chemical bond approach and average density of the composition.

2- According to the mean values of Avrami indices, $\langle n \rangle$, the two crystalline phases ($\text{Se}_{7.68}\text{Te}_{0.32}$, S_5Se_4) which are

formed during crystallization process of $\text{Se}_{85-x}\text{Te}_{15}\text{S}_x$ have surface nucleation, one dimensional growth from surface to the inside.

3- The diffractograms of the transformed material after the crystallization process suggest the presence of microcrystallites of two phases of $\text{Se}_{7.68}\text{Te}_{0.32}$ and S_5Se_4 for ternary crystallized phases in all the composition of $\text{Se}_{85-x}\text{Te}_{15}\text{S}_x$.

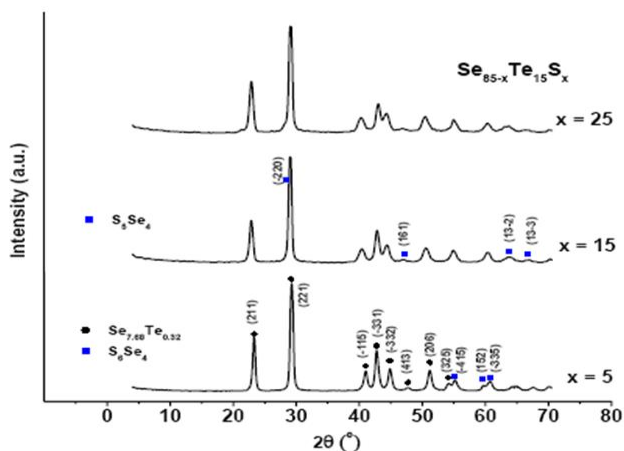


Fig. 14: Diffractogram of $\text{Se}_{85-x}\text{Te}_{15}\text{S}_x$ ($x = 5, 15, 25$) chalcogenide glass for two crystalline phases

References

- [1] S. A. Khan, F.S. Al-Hazmi, A.S. Faidah, A.A. Al-Ghamdi, *Current Applied Physics*, 9 (2009) 567.
- [2] M. Nakamura, Y. Wang, O. Matsuda, K. Inoue, K. Murase, *J. Non-Cryst. Sol.*, 740 (1996) 198.
- [3] L. Men, F. Jiang, F. Gan, *Mater. Sci. Eng.*, B 47 (1997) 18.
- [4] R. V. Woudenberg, *Jpn. J. Appl. Phys.*, 37 (1998) 2159.
- [5] T. Babeva, D. Dimitrov, S. Kitova, I. Konstantinov, *Vacuum*, 58 (2000) 496.
- [6] V. I. Mikla, I. P. Mikhalko, V.V. Mikla, *Mater. Sci. Eng.*, B 83 (2001) 74.
- [7] A. S. Maan, D. R. Goyal, *Chalcogenide Letters*, 4(8) (2007) 89.
- [8] A. K. Kolobov, J. Tominaga, *J. Optoelectron. Adv. Mater.*, 2002, 4 (3), 679.
- [9] S. A. Khan, M. Zulfequar, M. Husain, *Vacuum*, 72 (2003) 291.
- [10] E. R. Shaaban and S. H. Mohamed, *J. Thermal Anal.* 107 (2012), p. 617.
- [11] A. Goel, D. U. Tulyaganov, A. M. Ferrari, E. R. Shaaban, A. Prange, F. Bondioli, J. M. F. Ferreira, *Journal of the American Ceramic Society*, 93 (2010) 830.
- [12] A. Goel, D. U. Tulyaganov, M. J. Pascual, E. R. Shaaban, F. Muñoz, Z. Lü, Z., J. M. F. Ferreira, *J. Non-Cryst. Solids* 356, (2010) 1070.

- [13] J.L. Cadenas-Leal, J. Vazquez, D.G. Barreda, P.L. Lopez-Aleman, P. Villares and R. Jimenez-Garay, *Thermochim. Acta* 484 (2009) p.70.
- [14] T. Spassov, S. Todorova and V. Petkov, *J. Non-Cryst. Solids* 35 (2009) p.51.
- [15] A. Goel, D. U. Tulyaganov, D. U. Tulyaganov, J. M. F. Ferreira, *Journal of the American Ceramic Society* 91(2008) 2690.
- [16] A. Giridhar and S. Mahadevan, *J. Non-Cryst. Solids* 51 (1982) 305.
- [17] N. Afify, *J. Non-Cryst. Solids* 128 (1991) p.279.
- [18] M.J. Strink and A.M. Zahra, *Thermochim. Acta* 298 (1997) 179.
- [19] H. E. Kissinger, *Anal. Chem.* 29 (1957) 1702.
- [20] E. R. Shaaban, I. Kansal, M. Shapaan and J. M. F. Ferreira, *J. Thermal Anal.* 98 (2009) 347.
- [21] W. H. Zachariasen, *J. Am. Chem. Soc.* 54 (1932) 3841.
- [22] A. F. Loffe and A. R. Regel, *Prog. Semicond.* 4 (1960) 239
- [23] V. Sadgopam and H. C. Gotos, on the relationship of semiconductors compounds properties and the average heat of atomization, *Solid State Electron.* 8(1965) 529.
- [24] W A Johnson and K F Mehl, *Trans. Amer. Inst. Mining Eng* 135 (1981) 315.
- [25] M. Avrami, *J. Chem. Phys* 7 (1939) 1103; 8 (1940) 212; 9 (1941) 177.
- [26] C. Wagner, P. Villanes, J. Va'zquez, R. Jirnenex-Caray, Some methods for kinetic studies of non-isothermal crystallization in $\text{Sn}_{0.08}\text{As}_{0.26}\text{Se}_{0.66}$ alloy. *Mater Lett.* 19 (1993) 370.
- [27] E. R. Shaaban, I. S. Yahia and M. Fadel, *J. Alloys Comp.* 469 (2009), 427
- [28] A. Arora, A. Goel, E. R. Shaaban, O. P. Pandey and J. M. F. Ferreira, *Physica B:* 403 (2008) 1738.
- [29] A. Goel, D. U. Tulyaganov, I. K. Goel, E. R. Shaaban and J. M. F. Ferreira, *J. Non-Cryst. Solids* 355 (2009) 193.
- [30] E. R. Shaaban, M. Y. Hassaan, A. G. Mostafa and A. M. Abdel-Ghany, *J. Alloys Comp.* 482 (2009) 440.
- [31] E. R. Shaaban, M.T. Dessouky and A. M. Abousehly, *Philos. Mag.* 88 (2009), p. 1099.
- [32] N. Mehta, K. Singh and A. Kumar, *Physica B* 404 (2009) 1835.
- [33] A. Arora, E.R. Shaaban, K. Singh and O. P. Pandey, *J. Non-Cryst. Solids* 354 (2008) 3944.
- [34] E. R. Shaaban, H. A. Elshaikh and M. M. Soraya, *Int. J. New. Hor. Phys.* 1 (2014) 9.
- [35] K. Matusita, S. Saka, *J. Non-Cryst. Solids*, 38/39 (1980)
- [36] S. Mahadevan, A. Giridhar and A. K. Singh, *J. Non-Cryst. Solids*, 88 (1986) 11.